The Fourth IEEE RAS/EMBS International Conference
on Biomedical Robotics and Biomechatronics
Roma, Italy. June 24-27, 2012

A Camera Positioner Driven by Muscle-Like Actuation

Joshua Schultz[1] and Jun Ueda[2]

***Abstract*— Numerous camera positioning mechanisms exist, but their actuation has little in common with the human eye whose motion they are meant to replicate. Piezoelectric cellular actuators, a novel biologically inspired technology, have much more in common with the recti muscles that position the human eye than traditional actuators have. This work explains how to select multi-layer nested compliant strain amplification mechanisms that can scale up the displacement of piezoelectric stacks to the range of the ocular positioning system. The resulting actuators are deployed on a working single degree-of-freedom device.**

I. INTRODUCTION

The human eye is a remarkable, yet curious device: It enables the brain to perceive large amounts of information quickly, yet not all regions of space are perceived equally. Objects near the gaze direction, or fovea, receive the most attention, a lesser amount of information is gathered about objects in the remainder of the field of view, and some objects are out of the field of view and are not perceived. In this way, the brain is not overwhelmed by information that is not of interest. Because the area of interest may change rapidly, the eye can be reoriented with astounding performance by 6 lightweight recti muscles.

The recti muscles are contractile, compliant actuators that are activated in discrete steps by neural impulses. In this paper, we present a single-degree of freedom camera positioner, shown in Fig. 1, which can be used to understand the performance and control of a biologically inspired actuator technology that has much in common with human muscle. It is also a lightweight, high speed device. Each muscle-like actuator consists of a piezoelectric material and a nested hierarchical set of strain amplifying mechanisms. We present a mathematical formalism that can be used to predict the performance of and select the geometry of complicated nested structures of this type, using the design of the camera positioning mechanism's actuators to demonstrate the concepts. Eventually actuators of this type will be used to drive a 3 degree-of-freedom device that captures the kinematics and performance of the human eye.

This research was supported by NSF grant: Cyber-Physical Systems ECCS-0932208. Mr. Schultz is partially supported by a scholarship from the Achievement Rewards for College Scientists (ARCS) foundation.

[1]J. Schultz is with the Woodruff School of Mechanical Engineering, Georgia Institute of Technology, Atlanta, GA, 30332 USA joshua.schultz@gatech.edu

[2]J. Ueda is with the Woodruff School of Mechanical Engineering, Georgia Institute of Technology, Atlanta, GA, 30332 USA jun.ueda@me.gatech.edu

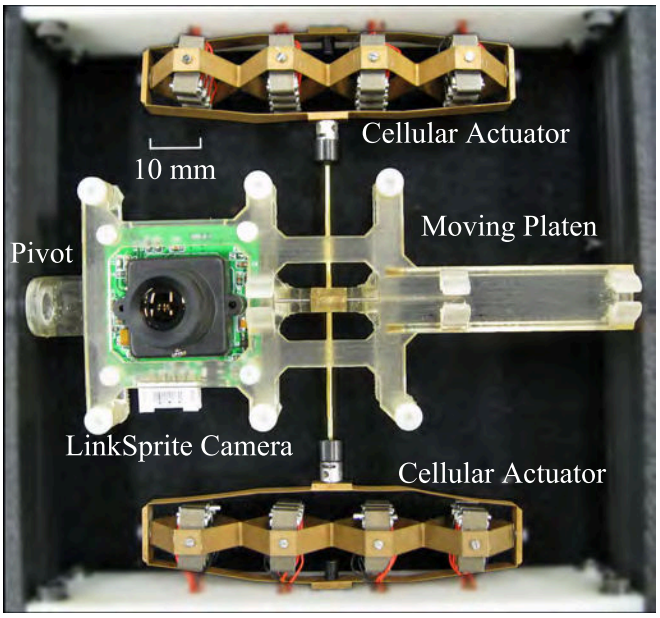

Fig. 1. Camera positioning mechanism

II. MOTIVATION

A. Automatic Camera Positioners

Most camera positioners use heavy traditional servomotors. Several notable examples exist which use non-traditional actuators. The spherical pointing motor [1],[2] consists of three sets of orthogonal windings and a permanent magnetic rotor mounted on a gimbal, which can be oriented by appropriately energizing the three coils. Chirikjian and Stein propose a spherical stepper motor which uses close packing of various semi-regular circular packings on a ferromagnetic sphere and coils [3]. The coils have a different packing pattern than the sphere, and as a result, the mechanism can reach a large finite set of final positions. The method of determining a proper step sequence to reach a given position is presented.

B. Human Ocular Motion

While these mechanisms represent unique and creative solutions to camera positioning, they have very little to do with how the human eye moves. The human eyeball, or globe, is oriented by means of antagonistic pairs of recti and oblique muscles. The range of achievable orientations follows Donders' Law and Listing's law, both for saccadic motion and smooth pursuit [4]. Cannata and Maggiali [5] maintain that antagonistic pairs of contractile actuators with insertion points into the globe are key to the eye's kinematics.

978-1-4577-1198-5/12/$26.00 ©2012 IEEE

Cannata and Maggiali's eye is a cable-driven mechanism actuated by traditional servomotors. In actuality, eye muscles consist of a finite number of on-off motor units, or collection of muscle fibers innervated by a particular motor neuron. Cytoskeletal tissue couples the active acto-myosin filaments to the load. Several researchers claim that this property allows muscles to function well in unstructured environments, since the elasticity of the muscle tends to return to a stable equilibrium when perturbed. Muscles are controlled by *recruitment*, whereby the nervous system increases or decreases the number of motor units active to increase or decrease the amount of actuation. Each individual motor unit can only be on or off; it cannot be proportionally controlled [6].

A cable-driven eye may be able to enforce the eye's kinematics, but rigid servomotors permit researchers to neither understand nor test hypotheses related to the neurological basis for eye motion, because they do not incorporate this concept of motor units. Some measure of "flexibility" can be implemented in software using traditional actuators, but it depends largely on having a continuously variable control signal and it does not elucidate how flexibility can be maintained with quantized actuation corresponding to neural recruitment phenomena. A camera positioning mechanism driven by contractile muscle-like actuators will result in a high-bandwidth eye, since they add little inertia, and do not suffer from velocity saturations and backlash as do traditional servomotor drives.

In the remaining sections of the paper, we will present a single degree-of-freedom camera positioner driven by the novel *cellular actuator* technology, which uses a contractile ceramic to generate motion. Unlike piezoelectric bimorph and unimorph actuators, it actuates along a straight line, and can be fabricated using hardware and equipment that is widely available. Like human muscle, its motion is an aggregation of on-off units coupled by a hardware flexibility. In the future, we plan to deploy these actuators on a multi-degree-of-freedom Donders-Listing compatible positioner.

III. CELLULAR ACTUATORS

Cellular actuators [7] consist of a number of lead zirconate titanate (PZT) ceramic stacks and a deformable amplification mechanism. When a voltage is applied to a piezoelectric material, it undergoes a mechanical strain, however, this strain is too small to be useful in robotic applications. The PZT stack applies a load to the amplification structure at the input, which due to the geometry of the mechanism results in a larger displacement at the output. This technique has been used successfully for planar grippers [8]. Cellular actuators use a simple rhomboid geometry and are modular devices. The rhomboid has a major diagonal, aligned with the PZT stack actuation direction and a minor diagonal, aligned with the output direction. The result is a larger output displacement, but smaller output force. Compliant mechanisms such as rhomboidal strain amplifiers transmit an action from the input to the output, but also transmit an action from the output to the input. For this reason, they are

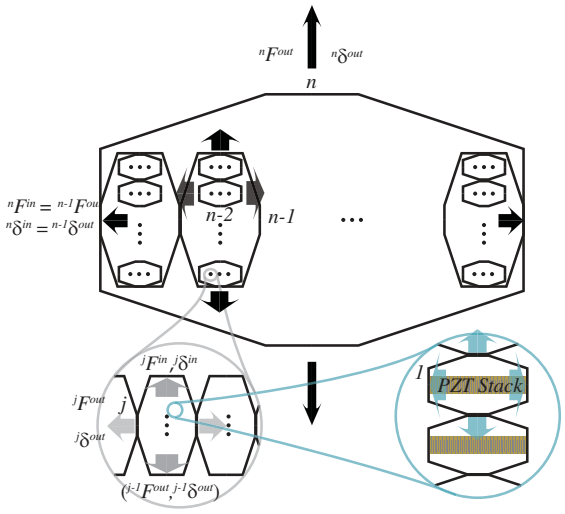

Fig. 2. Hierarchical nested mechanisms

modeled well by two-port network circuit models, which are described by

$$\begin{bmatrix} {}^{j}F^{in} \\ {}^{j}F^{out} \end{bmatrix} = \begin{bmatrix} {}^{j}s_1 & {}^{j}s_3 \\ {}^{j}s_3 & {}^{j}s_2 \end{bmatrix} \begin{bmatrix} {}^{j}\delta^{in} \\ {}^{j}\delta^{out} \end{bmatrix}, \qquad (1)$$

where ${}^{j}F^{in}$,${}^{j}F^{out}$ is the force at the input and output respectively, ${}^{j}\delta^{in}$,${}^{j}\delta^{out}$ are the displacements at the input and output, respectively. ${}^{j}s_1$, ${}^{j}s_2$, and ${}^{j}s_3$ are functions of material and geometric properties, and the matrix in (1) is positive definite. The leading superscript, j, denotes the rhomboid's position in the hierarchy, which consists of n "layers". In theory, a rhomboid can be designed to produce ${}^{j}s_1$, ${}^{j}s_2$, and ${}^{j}s_3$ that give any level of tradeoff desired, but certain factors limit this. These include internal interferences under deformation, manufacturing constraints, and buckling on thin sections. A solution is to use *successive layers of nested rhomboids* [7], each of which may include series-parallel combinations. A schematic of this mechanism-within-a-mechanism design concept is shown in Fig 2. The PZT stacks themselves form the innermost layer (layer 0). Once a good overall force-displacement tradeoff is achieved, cellular actuators can be combined in series and parallel combinations in order to have the stroke and maximum force required for the task.

Although PZTs can be controlled proportionally by varying the voltage, they are subject to hysteresis and thus require complicated drive electronics. When many stacks are available, reasonable resolution can be obtained by operating each stack in an on-off manner and simply choosing how many stacks to activate, avoiding these issues. In this way, collections of cellular actuators or cellular actuators with several stacks per "cell" share principles in common with muscles; their action is a sum of the individual units recruited and their effects are linked by an elastic medium.

IV. SINGLE-DEGREE-OF-FREEDOM-DEVICE

Although the ultimate goal of this research is a three-degree-of-freedom Listing-Donders compatible camera po-

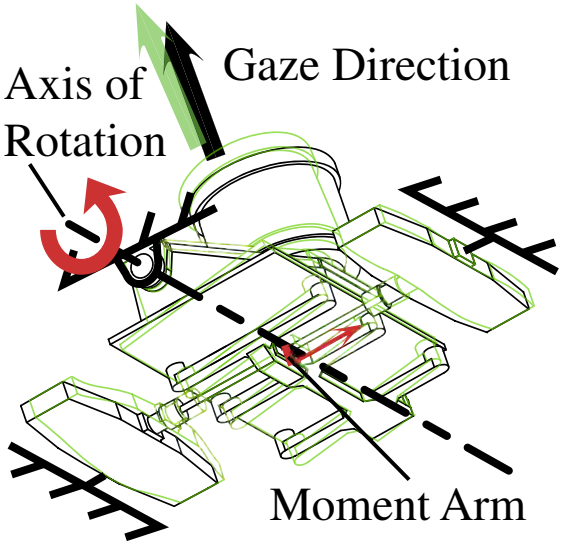

Fig. 3. Positioner centered (black) and reoriented (green)

sitioning mechanism, it is instructive to build and test a single-degree-of-freedom-device, shown in Fig. 1. This will allow us to verify recruitment-based control algorithms and review actuator performance independently of the kinematic and design challenges of a 3 degree of freedom device, which will require some sort of low-friction ball or gimbaled joint. The operation of the camera positioning device is illustrated in Fig 3.

The camera positioner supports a LinkSprite LS-Y201 camera. Since the goal is for the device to have performance similar to the human eye, it should have a working angle of $\pm 25^\circ$ (consistent with the linear region of human eye motion [9]). It should be capable of completing saccadic motions throughout its range within 50 ms [10]. The working range of the positioner is directly related to the actuator's free displacement (displacement of the actuator when no external force is applied). The saccade speed can be related to the actuator's blocked force (force applied by the actuator when no displacement occurs) and the inertia of the camera mechanism. With a moment arm of 5.84 mm, an antagonistic configuration, and adding a safety factor to avoid operating at the extremes of displacement (where the force capability is near zero), our desired free displacement comes out to be 8 mm.

Control and positioning is performed by a National Instruments NI cRIO-9024 device, which includes an embedded processor and 40 MHz FPGA. Switching signals are generated by an NI 9401 module with a 100ns resolution. Because PZT requires a high drive voltage, switching signals from the NI 9401 are sent to a custom switching circuit that uses Avago ASSR302-C solid state switching ICs to connect each individual stack to 150V or ground. The circuit is equipped with an electronic delay to enforce a "break before make" condition on the switch to prevent damage. The switching delay is nominally 80 μs. When the controller indicates that a given input should be recruited, the PZT stack will be connected to 150V. In order to release a given input, both ends of the PZT stack must be connected to ground so the charge stored can run into the ground plane. For this reason, simply disconnecting the PZT is not sufficient and both bridges of the ASSR302C must be used to control a single input. The circuit performs this operation automatically and requires only one signal line per PZT stack.

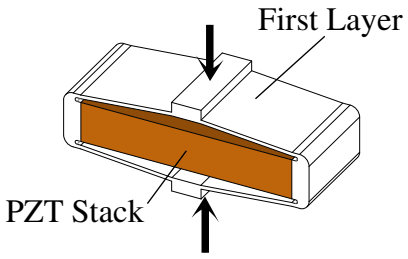

Fig. 4. PZT stack with a single layer of amplification

V. ACTUATOR DESIGN

A. Amplified PZT Base Units

To ease the implementation of the control algorithm [11], it is advantageous to have a number of active units that is a power of two. In addition, a somewhat coarse quantization was desired in order to show the algorithm's effectiveness. So each actuator in the antagonistic pair contains 16 PZT stacks. What we want to determine is:

- whether a nested compliant mechanism can be designed so that the action of 16 active units is sufficient to meet the desired free displacement
- if so, what blocked force can be achieved while also satisfying the desired free displacement

Because assembling the PZT stack into the innermost layer involves careful manufacturing techniques and closely held knowhow, we began with 16 amplified piezoelectric stacks from the Cédrat corporation, model APA50XS. The included rhomboidal amplification mechanism constitutes the first layer, i.e., the first layer is pre-determined. A PZT stack with a single layer of amplification is shown in Fig. 4. 16 of these units in series have a free displacement of 1.25 mm, which is well short of the desired value. So another layer of amplification is necessary.

B. Two Layer Actuator

To further increase the strain rate, the Cédrat units can be placed inside another rhomboidal mechanism, resulting in the two-layer structure shown in Fig. 5. This rhomboid will have parameters chosen for a good tradeoff. There are many possibilities for parameterization of a rhomboidal mechanism; we chose the set of parameters illustrated in Fig. 6. When multiple layers are being considered, each parameter will be given a subscript to denote the layer to which it applies, with the largest number referring to the outermost layer. Using a recursive matrix method based on

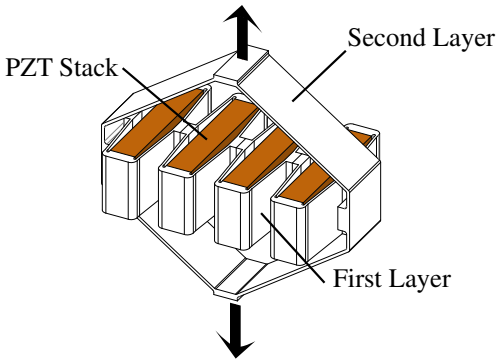

Fig. 5. PZT stack with two layers of amplification

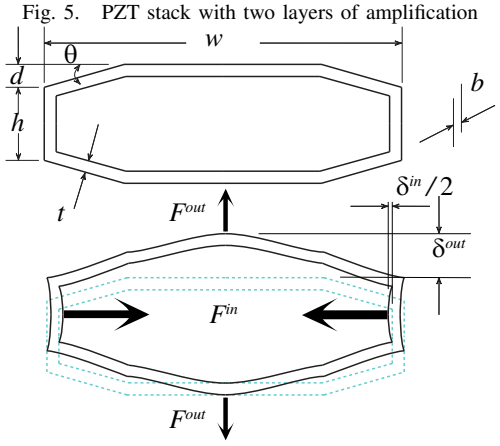

Fig. 6. Parameterization of a rhomboidal mechanism

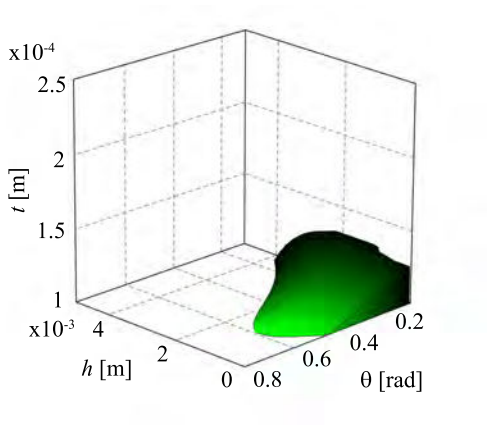

Fig. 7. Region in θ, h, t space where both good force and displacement properties can be achieved. Plot shown for 4 two-layer units in series with 4 Cédrat APA50XS units each. d is fixed at 1 mm. Displacement threshold is 4 mm total, force threshold is 0.5 N. Notice that the displacement threshold is only half of that required; the specification is not met by this configuration.

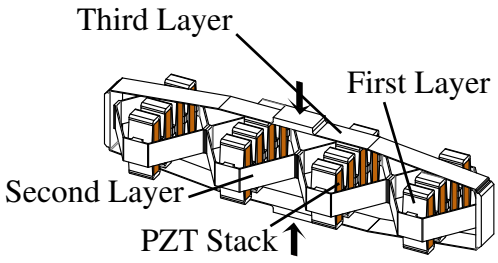

Fig. 8. PZT stack with a three layers of amplification

Castigliano's theorem, it is possible to obtain the immittance matrix elements ${}^{j}s_1$,${}^{j}s_2$, and ${}^{j}s_3$ as expressions of these parameters. This process is too involved to present here and is described in detail in another work, to be published soon. Once the immittance elements are determined, the free displacement and blocked force can be computed from (1) as:

$$ {}^{2}\delta^{free} = -\frac{{}^{2}s_3 \; {}^{1}F^{block}}{{}^{2}s_1 \; {}^{2}s_2 - {}^{2} \; s_3^2 + {}^{2} \; s_2 k_1} \tag{2} $$

$$ {}^{2}F^{block} = \frac{{}^{2}s_3^{1}F^{block}}{{}^{2}s_1 + k_1}, \tag{3} $$

where ${}^{1}F^{block}$ is the blocked force and k_1 is the stiffness of the APA50XS units.

Using Wolfram Mathematica's `NMaximize[]` routine, we maximized the free displacement subject to manufacturing and physical constraints. From this, we learn several things: other than interior of the small surface shown in Fig. 7, maximizing blocked force and free displacement seem to be competing goals, and free displacement falls off quickly with thickness, making it difficult to achieve a good tradeoff given manufacturing tolerances.

C. Three Layer Mechanism

For a given rhomboidal mechanism, the immittance matrix elements ${}^{j}s_1$, ${}^{j}s_2$, and ${}^{j}s_3$ are coupled, being analytical expressions of the same geometric parameters. This makes it difficult to achieve a favorable tradeoff between blocked force and free displacement. Optimization of a weighted function of force and displacement tend to return results that favor only one, with the other quantity being unsuitable. One might speculate that better tradeoffs can be achieved by exploiting the interplay between various layers, since the immittance matrices of each layer are largely decoupled from one another. In addition, rhomboidal mechanisms alternate between contractile and extensile outputs with each added layer, and a two-layer mechanism happens to be extensile. This can be overcome by using a concave "bow-tie" shaped mechanism [12], [13] but this topology may interfere with device being driven, and is not very compact. Since our goal is to create actuation that is similar to human muscle, we desire a compact, contractile mechanism. For all these reasons, we chose to explore the three-layer mechanism shown in Fig. 8, where we selected the second and third layer rhomboidal geometry.

The impedance of each layer affects the performance of the others; optimization of each of the layers cannot be conducted separately. The optimization problem has 9 parameters, resulting in much greater complexity. The general idea is to search the level surface corresponding to the desired free displacement for the maximum blocked force on the surface. Wolfram Mathematica's `NMaximize[]` routine is unable to solve this problem directly with 9 parameters, so

it proved necessary to break the search into steps, "guiding" the optimization routines to find an acceptable solution. This solution may not be globally optimal.

The first step maximized the lumped stiffness, or stiffness viewed from the output, of the two-layer unit, independently of the third layer. Then the third layer parameters were varied with the second layer geometry held fixed, maximizing free displacement. The resulting geometry serves as the initial condition to an unconstrained maximization on the free displacement. This resulted in a maximum free displacement of 12.9 mm, exceeding the specification.

The next step is to increase the blocked force. The natural procedure to arrive at a final design is to modify the geometry in the neighborhood of the maximum displacement and maximize the blocked force subject to the constraint that the free displacement be greater than 8 mm, possibly by constraint deletion since the free displacement constraint is a complicated function. While appealing, the numerical realities of the problem rendered it unsolvable using Wolfram Mathematica's optimization routines. Therefore, we proceeded by using a graphical search for a solution, varying two or three of the most significant parameters at a time.

D. Design Constraints

There are a number of constraints on the geometry imposed when optimizing a rhomboidal strain amplifying mechanism. The ones applicable to our case are summarized here; analogous constraints in the general case should follow logically from this example.

- Each rhomboid will be machined by wire EDM techniques, for which the minimum thickness t is 0.1 mm.
- The length of the angled section along the actuation direction d, must exceed the desired displacement of the amplification stage. Otherwise the rhomboid will fold up into a rectangle and the two-port model no longer applies. In this case the minimum d_3 was 2.4 mm.
- Although it is theoretically possible to have very small angles, there must still be a discernible angle when manufacturing tolerances, assembly misalignments, deformations during motion, and preloads are applied. We limited the angle of all stages to $6^\circ < \theta < 45^\circ$.
- The length of each layer in the output direction must match the length of the subsequent layer in the input direction. This was relaxed slightly between the second and third layers, allowing for a rigid "spacer" no longer than 5 mm on each side. Thus, w_3 was allowed to vary in a 10mm range.
- Each rhomboid must have its major axis along the input direction, i.e., $2d + h < w$.
- d, θ, and w must be chosen so that the geometry results in a simple convex polygon; anything else is considered a degenerate geometry and is not included.

In addition, the actuator must not impinge on itself when activated. For this reason, a rigid section was added to the middle of the third layer to make room for the first layer units.

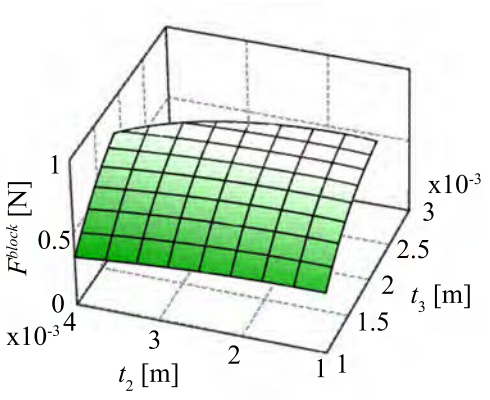

Fig. 9. Variation in (simulated) blocked force with t_3,t_2

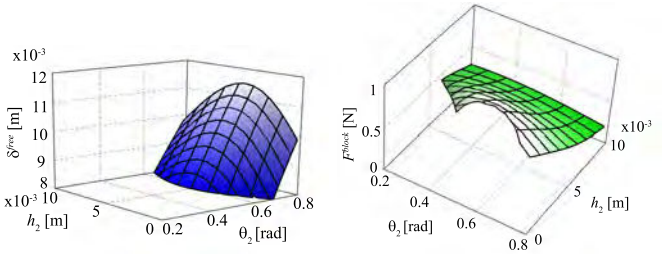

(a) Allowable Free Displacement (b) Blocked Force

Fig. 10. Variation in (simulated) performance with h_2,θ_2

VI. RESULTS

It turns out that the thickness of the outermost layer t_3 has the greatest effect on the free displacement/blocked force tradeoff, and high displacement actuators tend to have low t_3, θ_3 and d_3 values, with high w_3. These results are intuitive. A plot of blocked force vs. t_3 and t_2 is shown in Fig. 9. The surface is only plotted over regions that produce sufficient free displacement. This shows that the blocked force is greatest along the level surfaces where the displacement spec is just met.

The second layer parameter, t_2, affects the shape of this level surface, and the other second layer parameters do likewise. As can be seen in Fig. 10, the free displacement level surface is curved in h_2-θ_2 space, meaning that there is an internal point that represents the best force in this region. A correct second layer impedance is important to the design.

By plotting these surfaces for several t_2, we were able to arrive at the design shown in Table I. The resulting three layer actuator design has a free displacement of 8.1 mm and a blocked force of 0.907 N. By way of comparison, the Cédrat APA1000XL, the largest in their amplified piezoelectric stack actuator series, has a free displacement of 1.05 mm and has a footprint nearly 7.5 times larger than the three-layer actuator presented here. The APA100XL, like the other offerings from Cédrat, has only a single stage amplification mechanism.

VII. POSITIONER MOTION

Two instances of the piezoelectric cellular actuator designed in section V are placed in an antagonistic pair

TABLE I

FINAL DESIGN OF THREE-LAYER ACTUATOR

Quantity	Value	Units
d_3	2.40	mm
h_3	1.00	mm
θ_3	6	°
t_3	0.170	mm
w_3	68.8	mm
d_2	6.60	mm
h_2	3.00	mm
θ_2	35.1	°
t_2	0.250	mm
${}^3F^{block}$	0.907	N
${}^3\delta^{free}$	8.10	mm

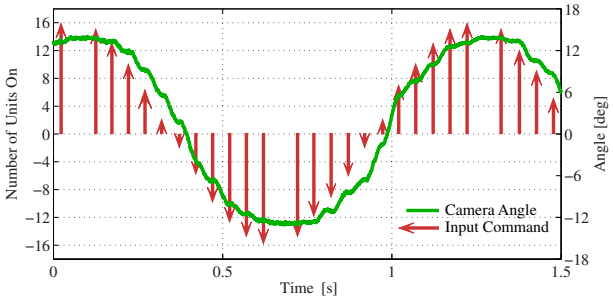

(a) Open loop trajectory

(b) Position I (c) Position II

Fig. 11. Motion of the camera positioner

arrangement. Fig. 11 shows the response of the camera to a quantized sinusoid with an amplitude of 16 units active. To reach an arbitrary position, a quantized control command [11], [14] would be substituted.

Theoretically, each actuator should move 4 mm (half of its free displacement) at maximum activation, exceeding the required angle of 25 degrees. Parasitic effects such as misalignments, residual stresses from manufacturing and assembly, and bearing friction limit this somewhat, so the displacement of this first prototype is less than predicted by the theoretical model.

VIII. CONCLUSION

This work presents an analysis of the force-displacement tradeoffs involved in the actuator design and shows how to find geometry that meets the requirements of a camera positioner. Actuator performance is demonstrated on a single degree-of-freedom device. It is compact enough to be used in autonomous robot navigation, indoor security, and humanoid applications. The cellular actuator, a biologically inspired actuation technology that uses a multi-stage hierarchical compliant mechanism to scale up the displacement of piezoelectric ceramic stacks, holds great potential to more accurately replicate human eye motion than do traditional actuators. Future work will involve implementation of this technology on a multi-degree of freedom Listing-Donders compatible device, applying open and closed loop control algorithms for positioning, and analysis of co-contraction phenomena.

REFERENCES

[1] B. Bederson, R. S. Wallace, and E. L. Schwartz, "Two miniature pan-tilt devices," in *IEEE Conference on Robotics and Automation*, 1992.

[2] ——, "A miniature pan-tilt actuator: The spherical pointing motor," *IEEE Transactions on Robotics and Automation*, vol. 10, no. 3, pp. 298–308, June 1994, three Orthogonal Coils on a Gimbal.

[3] G. S. Chirikjian and D. Stein, "Kinematic design and commutation of a spherical stepper motor," *IEEE/ASME Transactions on Mechatronics*, vol. 4, no. 4, pp. 342–353, December 1999.

[4] J. Crawford, J. Martinez-Trujillo, and E. Klier, "Neural control of three-dimensional eye and head movements," *Current Opinion in Neurobiology*, vol. 13, pp. 655–662, 2003.

[5] G. Cannata and M. Maggiali, "Models for the design of bioinspired robot eyes," *IEEE Transactions on Robotics*, vol. 24, no. 1, pp. 27–44, February 2008.

[6] E. N. Marieb, *Human Anatomy and Physiology*, K. Ueno, Ed. Benjamin Cummings, 2001, Texbook Definitive statement on motor units.

[7] J. Ueda, T. Secord, and H. Asada., "Large effective-strain piezoelectric actuators using nested cellular architecture with exponential strain amplification mechanisms," *IEEE/ASME Transactions on Mechatronics*, vol. 15, pp. 770–782, 2010.

[8] S.-C. Huang and W.-L. Chen, "Design of topologically optimal microgripper," in *IEEE International Conference on Systems, Man and Cybernetics*, 2008.

[9] W. Haustein, "Considerations on listing's law and the primary position by means of a matrix description of eye position control," *Biological Cybernetics*, vol. 60, no. 6, pp. 411–420, 1989.

[10] D. A. Robinson, "The mechanics of human saccadic eye movement," *the Journal of Physiology*, vol. 174, pp. 245–264, 1964.

[11] J. Schultz and J. Ueda, "Intersample discretization of control inputs for flexible systems with quantized cellular actuation," in *Proceedings of the ASME Dynamic Systems and Control Conference, Cambridge, MA*, September 2010.

[12] T. W. Secord and H. H. Asada, "A variable stiffness actuator with tunable resonance for cyclic motion tasks," in *IEEE International Conference on Robotics and Automation*, Kobe, Japan, May 2009, p. 176181.

[13] T. Secord and H. Asada, "A variable stiffness pzt actuator having tunable resonant frequencies," *Robotics, IEEE Transactions on*, vol. 26, no. 6, pp. 993 –1005, dec. 2010.

[14] J. Schultz and J. Ueda, "Experimental verification of discrete switching vibration suppression," *Mechatronics, IEEE/ASME Transactions on*, vol. PP, no. 99, p. 1, 2011.